Journal of The Electrochemical Society

The Electrochemical Society
Advancing solid state & electrochemical science & technology

OPEN ACCESS

Reduction of ZrO_2 during SNF Pyrochemical Reprocessing

To cite this article: Andrey Nikolaev *et al* 2021 *J. Electrochem. Soc.* **168** 036506

View the article online for updates and enhancements.

240th ECS Meeting
Oct 10-14, 2021, Orlando, Florida
Register early and save
up to 20% on registration costs
Early registration deadline Sep 13
REGISTER NOW

This content was downloaded from IP address 212.193.94.28 on 09/08/2021 at 08:00

Journal of The Electrochemical Society, 2021 **168** 036506

Reduction of ZrO_2 during SNF Pyrochemical Reprocessing

Andrey Nikolaev,[1,2] Andrey Suzdaltsev,[1,2,z] Olga Pavlenko,[1,2] Yuriy Zaikov,[1,2] Tatyana Kurennykh,[3] and Vladimir Vykhodets[3]

[1]*Institute of High-Temperature Electrochemistry UB RAS, 620137 Yekaterinburg, Russia*
[2]*Ural Federal University, 620002 Yekaterinburg, Russia*
[3]*Institute of Metal Physics UB RAS, 620108 Yekaterinburg, Russia*

Reduction of ZrO_2 by lithium during electrolysis of LiCl-KCl-Li_2O melt at 650 °C was studied using a set of physicochemical methods of analysis. Influence of ZrO_2 in the space near a molybdenum cathode on the kinetics of the cathode process was established. Possible variations of the electrode reaction associated with the zirconium reduction were proposed. The appearance of ZrO_2 in the cathode space resulted in consumption of reduced lithium and in increase in the potential relaxation time of the molybdenum cathode after cathode polarization. Long-term galvanic impulse electrolysis of LiCl-KCl-Li_2O melt at 650 °C was carried out using the molybdenum cathode which was immersed into the ZrO_2 powder. According to the X-ray fluorescence analysis as well as the method of nuclear reactions the reduction product was presented by the ZrO_2, Li_2ZrO_3, Zr_3O phases. Additionally, by alloying the reduction product with tin, the ZrO_2 reduction degree to metallic zirconium was estimated, which was close to zero. It was assumed that the main pathway for the appearance of the metallic zirconium in the ZrO_2 reduction product during electrolysis of the LiCl-KCl-Li_2O melt was direct electroreduction of dissolved zirconium in the melt.
© 2021 The Author(s). Published on behalf of The Electrochemical Society by IOP Publishing Limited. This is an open access article distributed under the terms of the Creative Commons Attribution Non-Commercial No Derivatives 4.0 License (CC BY-NC-ND, http://creativecommons.org/licenses/by-nc-nd/4.0/), which permits non-commercial reuse, distribution, and reproduction in any medium, provided the original work is not changed in any way and is properly cited. For permission for commercial reuse, please email: permissions@ioppublishing.org. [DOI: 10.1149/1945-7111/abe8be]

Manuscript submitted December 12, 2020; revised manuscript received February 13, 2021. Published March 4, 2021. *This paper is part of the JES Focus Issue on Molten Salts and Ionic Liquids II.*

Molten salts are promising media for the synthesis of materials and recycling the secondary wastes.[1–3] In particular, the use of melts based on lithium chloride suggests pyrochemical schemes for the reprocessing of spent nuclear fuel (SNF),[4–7] including the reduction of actinide oxides during the electrolysis of LiCl-Li_2O melt, electrorefining and electro-extraction of actinides in the LiCl-KCl molten eutectic. Much attention was paid to the reduction of a wide range of individual oxides during electrolysis of the LiCl-Li_2O melt. Moreover, outstanding interest was to the study of possibility to reduce oxidized nuclear fuel presented by actinide oxides (UO_2, PuO_2), rare-earth metal oxides (Nd_2O_3, CeO_2, La_2O_3, etc.) as well as ZrO_2.

Nowadays, the method of reprocessing oxide/oxidized or preoxidized SNF during the electrolysis of LiCl-Li_2O melts is proposed. This is possible due to the fact that the actinides oxides are reduced to metals by lithium, while the oxides of rare earth metals predominantly remain in the oxide phase.[8–10] The issue of ZrO_2 reduction to zirconium is still not clear. In Ref. 11, the experimental results regarding the reduction of ZrO_2 and its mixtures with UO_2 and PuO_2 during electrolysis of the LiCl-Li_2O melts were presented in dependence on the Li_2O content in the melt. It was revealed that regardless the ZrO_2 content in the initial mixtures, the UO_2 and PuO_2 oxides can be completely reduced to uranium and Plutonium, and the ZrO_2 undergoes only partial reduction to metal, despite the same thermodynamic probability of the UO_2 and ZrO_2 reduction reactions by lithium:

$$1/2UO_2 + 2Li = 1/2U + Li_2O;$$
$$\Delta G^0_{650\ ^\circ C} = -13.38\ \text{kJ mol}^{-1}, \quad [1]$$

$$1/2ZrO_2 + 2Li = 1/2Zr + Li_2O;$$
$$\Delta G^0_{650\ ^\circ C} = -13.80\ \text{kJ mol}^{-1} \quad [2]$$

It was suggested[11] that one of the reasons for the incomplete reduction of ZrO_2 was the formation of the lithium zirconates, although it was indicated in Refs. 12–14, based on the X-ray phase and spectral analysis, that both ZrO_2 and Li_2ZrO_3 are partially reduced to metallic zirconium.

On the other hand, in studies related to the behavior of the oxygen-conducting ZrO_2-based diaphragms in the LiCl-Li_2O and LiCl-Li_2O-Li melts, only the formation of lithium zirconates was found.[15–18]

The results disagreement in these works can be caused by the application of different methods in order to determine the metallic zirconium in the recovered products. For example, in Ref. 11, the cathode products were dissolved in a mixture of nitric and hydrofluoric acids, while in Refs. 11–14 the diaphragms were washed only by distilled alcohol or water. In the case of dissolution in acidic aqueous solutions, ZrO_2 as well as the lithium zirconates, can undergo partial dissolution; in Refs. 11–14, the results of determining the degree of the ZrO_2 reduction can be overestimated. This is confirmed by the values of the zirconium oxide solubility in aqueous solutions at a temperature of 25 °C and above.[19,20] The second reason for the detection of the metallic zirconium in the products of the ZrO_2 reduction by lithium may be due to unaccounted processes of direct electrochemical reduction of:

- zirconium ions formed during dissolution of ZrO_2 in the LiCl melt containing Li_2O;
- electron-conducting non-stoichiometric mixtures of Li-Zr-O according to the mechanism of "electro-deoxidation".[21–23]

From the above stated it follows that the study of the ZrO_2 reduction specifically, as well as its mixtures with actinide oxides during electrolysis of melts based on the LiCl-Li_2O system, is still challenging. Moreover, special attention should be paid to the accuracy of method used for determination of the recovered product.

In this work, we studied the degree of the ZrO_2 secondary reduction in the cathode space during electrolysis of the LiCl-KCl-Li_2O melt by means of a set of physicochemical methods. Over time, the LiCl-KCl-Li_2O melt can be also used for the reduction of oxides by lithium at low temperatures as well as low activities of lithium and oxygen ions in the melt. These entities can act as regulators for the selective reduction of the SNF components. The experiments were performed at 650 °C in order to compare the obtained results with the data of the ZrO_2 reduction in the LiCl-Li_2O melt at the same conditions.

[z]E-mail: suzdaltsev_av@ihte.uran.ru

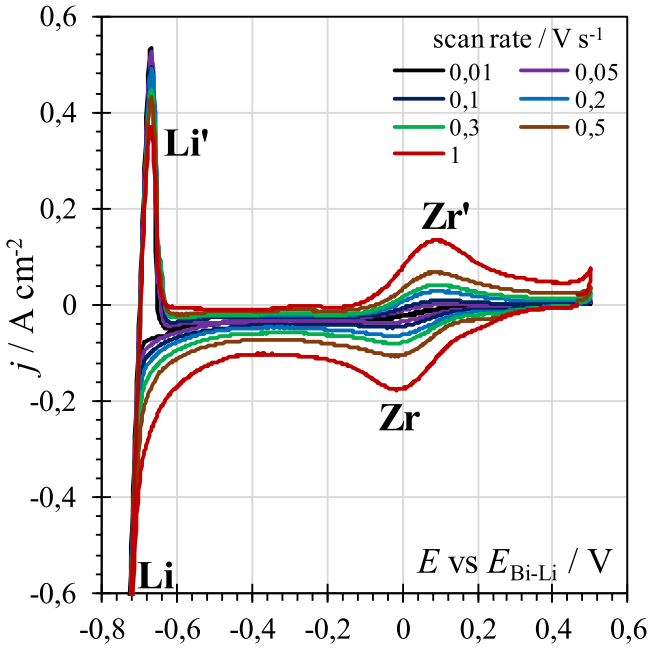

Figure 1. CVs obtained on the Mo cathode in the LiCl-KCl-(1.5 wt%)Li_2O melt with the presence of ZrO_2 at 650 °C and at the potential sweep rate of 0.01–1 V s^{-1}.

Experimental

Electrolyte preparation.—The LiCl and KCl individual chlorides were taken for preparation. First, they were gradually heated under vacuum, melted in argon, and then subjected to zone recrystallization.[24] Previously, the LiCl-KCl melt was saturated with respect to Li_2O.[25] This mixture (with known amount of Li_2O) was used for the lithium oxide addition to the LiCl-KCl electrolyte under investigation. All operations, including storage of salts, experiments performance, as well as auxiliary operations were carried out in a dry argon box. The ZrO_2 powder with an average particle size of 20–40 μm was used.

Electrochemical cell.—Electrochemical measurements and electrolysis tests were carried out in a container made of MgO filled with the LiCl-KCl-(1.5 wt%) Li_2O melt at 650 °C. The container was placed in a quartz retort covered with a fluoroplastic lid; thus, the melt was isolated from the box atmosphere. A counter electrode (oxygen-evolving anode based on NiO ceramics[7]), two working molybdenum electrodes with the same geometric surface of 1.27 cm^2 (standard Mo and the Mo/ZrO_2 electrode immersed into the MgO crucible with ZrO_2 powder), a thermocouple and a Bi-Li quasi reference electrode (QRE) in a porous MgO diaphragm were fixed in the lid. The Bi-Li alloy was obtained by the deposition of lithium on the liquid bismuth in the LiCl-KCl-Li_2O melt. The lithium content in the obtained Bi-Li alloy was analyzed by ICP. The Li content was found to be 15 wt%. The potential stability of such electrode during long-term tests was proved in Ref. 26.

Electrochemical measurements.—The PGSTAT AutoLab 320 N with NOVA 1.11 software (The MetrOhm, Netherlands) was applied for conducting the electrochemical measurements and electrolysis. The melt temperature was measured by means of Pt/PtRh thermocouple and USB-TC01 module (National Instruments, USA). The electrolysis was performed in an impulse galvanostatic mode, which provided the release of lithium and fixation of the electrode potential during a short-term (60 s) current cut-off. When electrolysis was completed, a cathode in the shape of spiral was positioned at the bottom of the MgO-crucible. The ZrO_2 powder was added to the crucible.

The analysis of reduced product.—After the electrolysis was completed, the reduced ZrO_2 powder was removed from the MgO-crucible and washed many times in distilled alcohol. In order to determine the composition of reduction products, a set of methods was applied: inductively coupled plasma atomic emission spectrometry (Optima 4300 DV instrument, Perkin Elmer) with a detection limit for the analyzed elements of 0.001–0.0001 wt%; X-ray fluorescence analysis (Supermini 200 device, Rigaku); carbothermal reduction of oxide with subsequent analysis of the absorption of infrared radiation (OH 836 analyzer, LECO).

Nuclear reaction analysis.—Since reduced ZrO_2 contained lithium and oxygen, the nuclear reaction analysis (NRA) technique was additionally used to determine their content. This method was applied for the accurate measurement of the isotopes concentration of light elements in solids. The oxygen and lithium concentrations were determined using 2 MV van de Graaf generator, which provides nuclear reactions $^{16}O(d,p_0)^{17}O$, $^{6}Li(d,p_0)^{7}Li$ and $^{7}Li(d,p)^{8}Li$ in the samples.[27,28] The energy of the deuteron beam was 650 keV. Nuclear reaction spectra were recorded using silicon surface-barrier detector with an area of 1 cm^2. The irradiation dose of the samples was measured by means of secondary monitor with an error of about 1.5%. Powder particles were pressed into an indium plate. As a result, a layer with the thickness of at least 2 μm was formed near the outer surface of the sample, containing only oxide particles. The flat surface of the samples was set perpendicular to the axis of the incident beam. The procedure of comparing the sample spectrum and the spectrum of the etalon sample with clearly defined concentrations of oxygen and lithium was used in order to calculate the values of the oxygen and lithium concentrations. The initial ZrO_2 powder (67 at.% oxygen) and Li_2ZrO_3 (33.3 at.% lithium) were served as etalon samples.[29] The concentrations were calculated using tabulated data according to the stopping power of the elements.

Alloying with tin.—The reduction product alloying with tin was selected for the assessment of the ZrO_2 reduction degree. The tin was chosen as a solvent, interacted with zirconium but not with ZrO_2. Previously, a similar technique was tested for the separation of the cathode product from the salt.[30] In addition to the reduction product, the initial ZrO_2 powder and lithium zirconate Li_2ZrO_3 were also melted with tin. The melting was carried out in a glassy carbon crucible under a layer of LiCl-KCl salt flux at 700 °C for two hours.

Results and Discussion

Cathode process.—The stability of potential difference between the QRE and the Mo electrode was estimated before carrying out the electrochemical measurements. It was 0.605 ± 0.003 V for 4 h. Cyclic voltamogramms (CVs) obtained on the pure Mo electrode in the LiCl-KCl melt with the addition of 1.5 wt% Li_2O at 650 °C are shown in Fig. 1. A wave of the lithium electroreduction in the potential region more negative than −0.65 V with respect to the QRE potential and a peak of the lithium anodic dissolution are observed in the CVs. The cathode and anode peaks of the OR process can be seen at potentials 0 and 0.1 V, respectively. With an increase in the potential sweep rate from 0.01 to 1 V s^{-1} the current density of the cathodic peak rises from 27 to 178 mA cm^{-2}, while the peak potential does not change. The cathodic peak can be caused by the reduction of zirconium ions, which could appear in the melt due to the dissolution of ZrO_2 powder from the Mo/ZrO_2 electrode, which is immersed in the melt. This assumption is confirmed, firstly, by the data of the atomic emission analysis of the samples, according to which the zirconium content in the melt reaches 0.08–0.09 wt% (0.13–0.15 wt% in terms of ZrO_2), and, secondly, by the experimental data related to the potential of zirconium electrodeposition from the LiCl-KCl-$ZrCl_4$ melts, which is 1.0–1.2 V more positive than the potential for the lithium

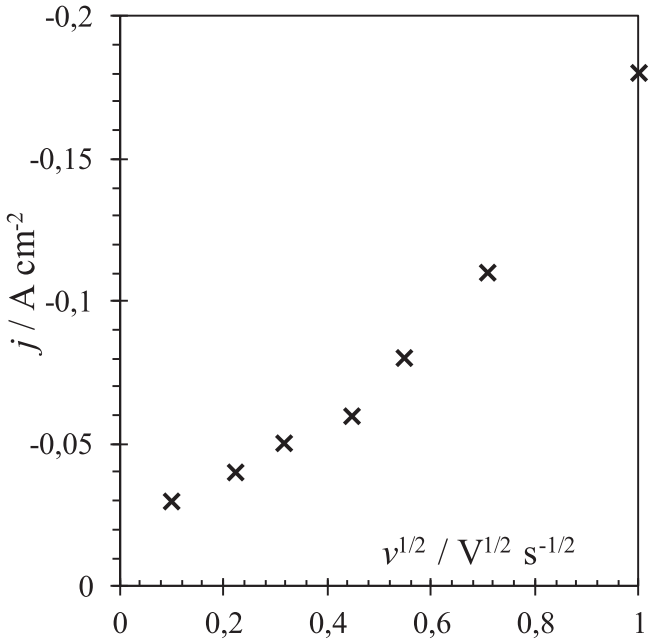

Figure 2. The dependence of the peak current density on the square root of the potential sweep rate for the Mo cathode in the LiCl-KCl-(1.5 wt%) Li_2O melt with the presence of ZrO_2 at 650 °C.

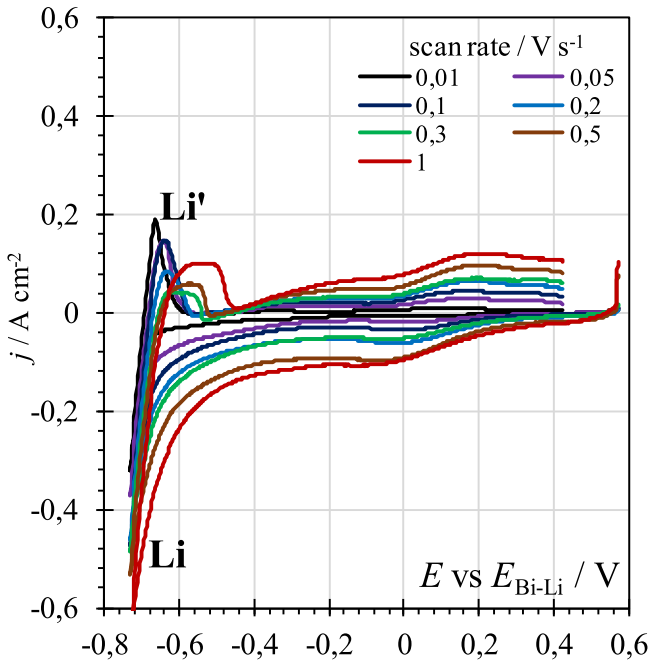

Figure 3. CVs obtained on the Mo/ZrO_2 cathode in the LiCl-KCl-(1.5 wt%)Li_2O melt with the presence of ZrO_2 at 650 °C and at the potential sweep rate of 0.01–1 V s^{-1}.

electroreduction.[31–34] The dissolution of ZrO_2 is facilitated by the presence of oxygen ions in the chloride melt.[35,36]

At the same time, a clear inflection is seen in the dependence of the peak current density on the square root of the potential sweep rate (Fig. 2), which may be due to the zirconium reduction to various reduced forms that are zirconium subchlorides.[31–34]

The CVs obtained under similar conditions on the Mo/ZrO_2 cathode are given in Fig. 3. Reasonably, one can note the similarity of the dependences obtained on the Mo and Mo/ZrO_2 cathodes, with exception of the following differences:

- instead of clear peaks of reduction and oxidation of zirconium, a wave blurred along the potential axis is observed;
- cathodic currents in the potential region before the release of lithium are higher for the Mo/ ZrO_2 electrode;
- the presence of ZrO_2 at the cathode reduces the peak current of the lithium anodic dissolution.

The last two effects indicate the consumption of the reduced form of lithium, for instance, as a result of the subsequent chemical reaction of the lithium zirconate formation.[1,37,38]

Similar results can be observed in the square-wave voltammograms (SWVs) obtained on Mo and Mo/ZrO_2 cathodes at the same conditions (Figs. 4 and 5). The SWVs were received at a potential reverse frequency from 2 to 200 Hz with potential shift step of 5 mV (correspond to the potential sweep rate from 0.01 to 1 V s^{-1}). The SWVs on the Mo cathode are characterized by a clear peak at a potential of about 0 V and a wave of lithium electroreduction at the potential more negative than −0.65 V (Fig. 4a). An increase in the potential reverse frequency leads to a rise in the total current signal in the SWVs, which is typical for the electrode process controlled by the diffusion of electroactive ions to the cathode.

The dependences of the relaxation of Mo cathode potential after the square-wave voltammetry measurements are presented in Fig. 4b. A plateau of lithium dissolution is noticed at a potential of −0.7 V. Then, the cathode potential shifts sharply to the potential region of about 0 V, whereas the dissolution wave of the reduced form of zirconium occurs within next 10–20 s. An increase in the amount of electricity passed through the cathode (decreasing the potential reverse frequency) leads to a rise in the dissolution time of both lithium and reduced form of zirconium. From the half-peak width ($W_{1/2}$, V) one can estimate the number of electrons (z) of the reaction at the potential of about 0 V, according to the expression:

$$W_{1/2} = 3.52RT/zF \qquad [3]$$

where R is the universal gas constant, $R = 8.314$ J K^{-1} mol^{-1}; T is temperature, K; F is Faraday number, $F = 96487$ C mol^{-1}. For frequencies of 100 and 200 Hz the number of electrons is close to 2, while for low frequencies it is closer to 1.

The ZrO_2 appearance near the cathode leads to a decrease in the peak current of the cathode process on the Mo/ZrO_2 cathode at the potential of about 0 V (Fig. 5a) and an increase in the cathodic current in the potential region up to the lithium deposition wave (from 0 to −0.65 V). In such case, the relaxation time of the Mo/ZrO_2 cathode potential increases (Fig. 5b) by more than an order of magnitude. Such effect can be explained by slow lithium removal from the oxide pores into the melt volume and/or the subsequent reduction of ZrO_2 by lithium. An increase in the cathodic current in the potential range before the lithium phase formation (positively than −0.65 V) indicates the consumption of the reduced lithium in reaction (2).

The chronopotentiogramms (CPs) obtained on the Mo and Mo/ZrO_2 cathodes in the studied melt at 650 °C, depending on the magnitude of the cathodic current pulse, are presented in Fig. 6. It can be seen that an increase in the cathode current impulse leads to the Mo and Mo/ZrO_2 cathodes potential shifting into the region of more negative potentials. An appearance of the ZrO_2 powder near the cathode leads to the increase in duration of the potential decay of the Mo/ZrO_2 cathode due to the reasons indicated above. Generally, one can note the consistency of the results for studying kinetics of processes occurred on the Mo and Mo/ZrO_2 cathodes obtained by different electrochemical methods of analysis.

Electrolysis of the LiCl-KCl-Li_2O melt.—During the long-term impulse electrolysis the potential of the Mo/ZrO_2 cathode under current smoothly shifted from −1.6 to −1.4 V (Fig. 7). At the moments of current interruption (1 min) its value corresponded to the potential of the lithium electrode (about −0.7 V). These observations are differed from the case when the UO_2 is reduced

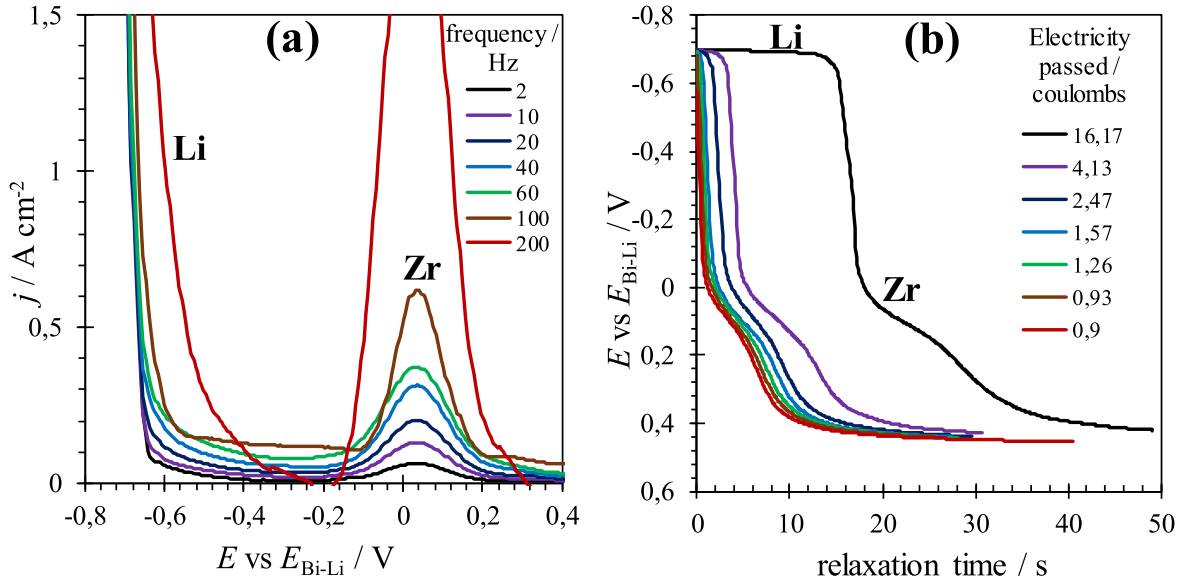

Figure 4. The SWVs (a) obtained on the Mo cathode in the LiCl-KCl-(1.5 wt%)Li_2O melt with the presence of ZrO_2 at 650 °C and at the potential reversal frequency of 2–200 Hz (scan rate 0.01–1 V s^{-1}). The amplitude is 50 mV. The Mo cathode potential relaxation dependences after polarization under conditions of SWVs (b).

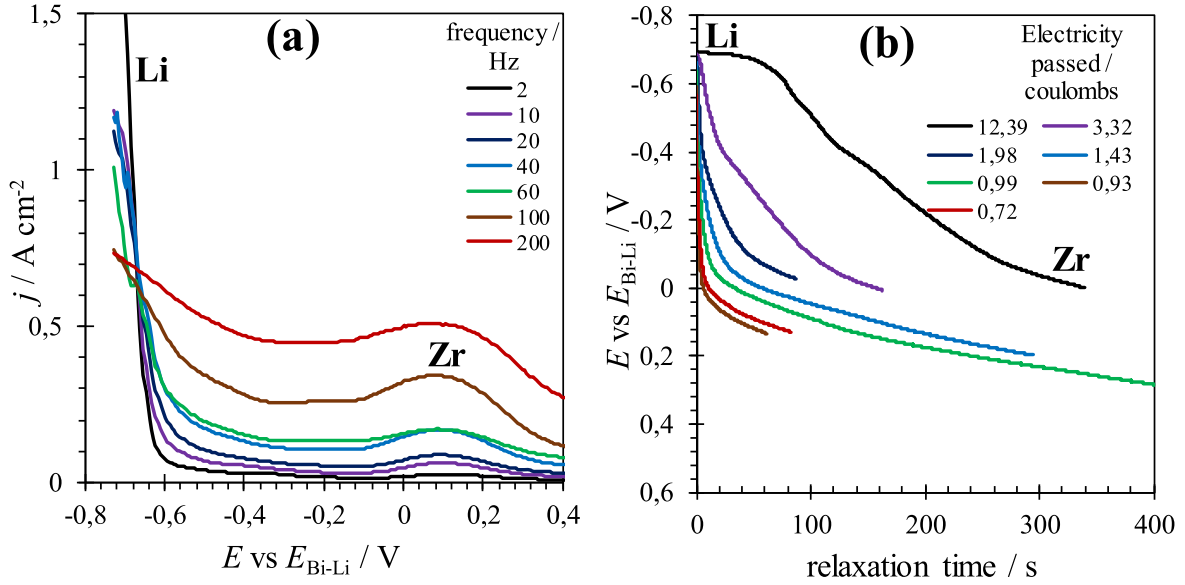

Figure 5. The SWVs (a) obtained on the Mo/ZrO_2 cathode in the LiCl-KCl-(1.5 wt%)Li_2O melt with the presence of ZrO_2 at 650 °C and at the potential reversal frequency of 2–200 Hz (scan rate 0.01–1 V s^{-1}). The amplitude is 50 mV. Mo/ZrO_2 cathode potential relaxation dependences after polarization under conditions of the SWVs (b).

by lithium during electrolysis of the LiCl-Li_2O-based melt. Namely, the cathode potential sharply shifts to the positive region and becomes equal to the potential of the uranium electrode.[39,40]

Thus, the consumption of the reduced lithium for the ZrO_2 reduction is typical only at the initial moments of electrolysis. During the long-term electrolysis, lithium accumulated as a separate phase and only a small amount of it consumed on the ZrO_2 reduction. This is confirmed by the results of electrolysis tests given below. In Fig. 8 the images of the MgO container with electrolyte after cooling, MgO crucible with reduction products, and a reduction product separated from the molybdenum cathode are presented. The following can be assumed as a result of electrolysis of the LiCl-KCl-Li_2O melt:

- the ZrO_2 powder in the layer near the cathode acquired a dark gray color;
- the MgO container and MgO crucible were partially reduced or impregnated with metallic lithium, as indicated by the change in their color from white to gray;
- a drop of lithium metal formed on the surface of the melt.

Analysis of the reduction products.—The analysis results of the reduced ZrO_2 powder composition obtained during the long-term electrolysis of the LiCl-KCl-(1.5 wt%) Li_2O melt at 650 °C can be seen in Figs. 9–11. According to the XRF analysis data, after washing from salts, the powder contained the phases ZrO_2, Li_2ZrO_3, Zr_3O, as well as residual KCl (Fig. 9).

According to the data of the carbothermal melting method, a decrease in the oxygen content from 26.3 ± 0.9 to 22.7 ± 0.7 wt% was determined in the ZrO_2 powder sample after reduction (Fig. 10). All these results indicate the reduction of ZrO_2.

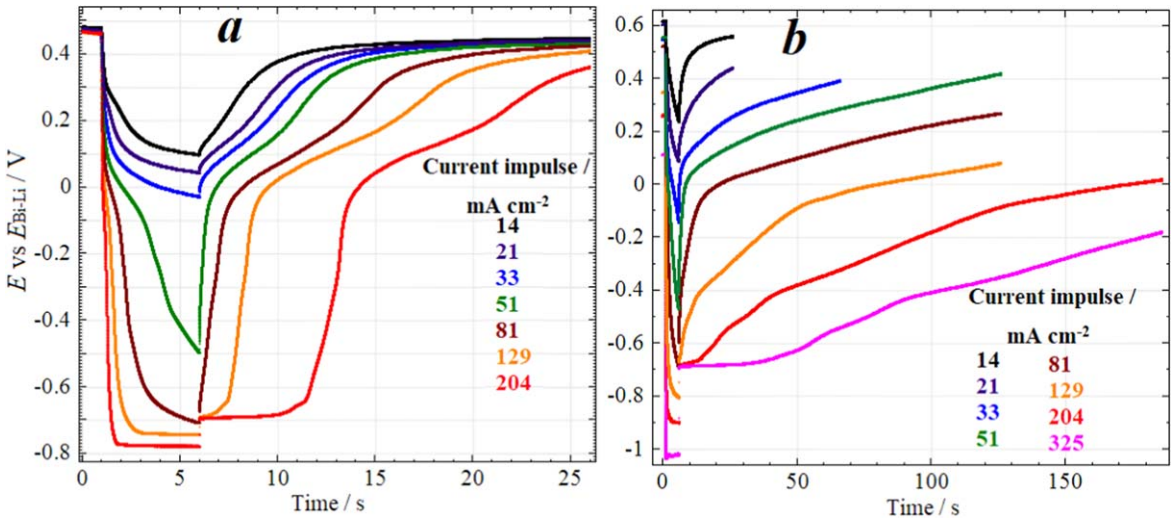

Figure 6. The CPs obtained on Mo (a) and Mo/ZrO_2 (b) cathodes in the LiCl-KCl-(1.5 wt%) Li_2O melt with the presence of ZrO_2 at 650 °C depending on the magnitude of the cathode impulse.

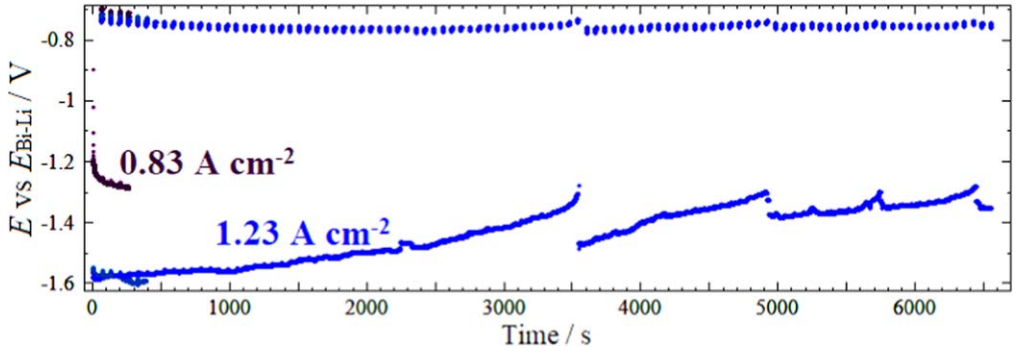

Figure 7. The change in the potential of the Mo/ZrO_2 cathode during impulse galvanostatic electrolysis of the LiCl-KCl-(1.5 wt%)Li_2O melt at 650 °C.

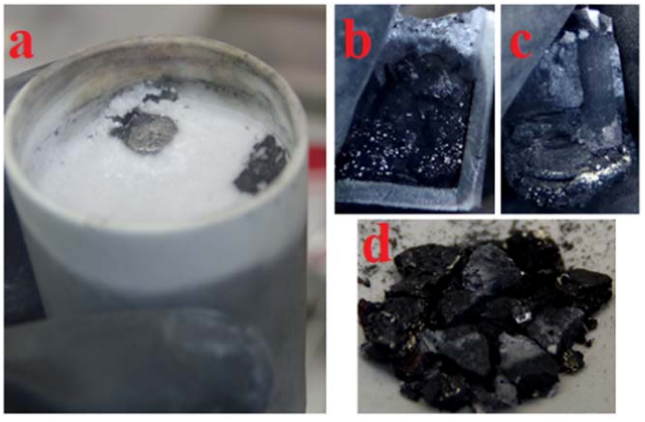

Figure 8. Images of the MgO container with electrolyte after cooling (a), MgO crucible with a reduction product (b), a cathode (c) and a reduction product (d) separated from the cathode after the electrolysis of the LiCl-KCl melt (1.5 wt%)Li_2O at 650 °C.

The spectra of the nuclear reaction's products with initial ZrO_2, Li_2ZrO_3, and with reduced ZrO_2 during electrolysis of the LiCl-KCl-Li_2O melt are presented in Fig. 11. It can be observed that the powder contained a significant amount of lithium. Since the spectrum of lithium was superimposed on the spectrum of oxygen, the oxygen concentration in the powder was estimated by subtracting the spectra. For an alternative assessment of the oxygen concentration an additional experiments were carried out with the irradiation of samples not with deuterons, but with protons, as a result of which the concentration of not only the ^{16}O isotope, but also ^{18}O was measured, while the reaction products from the ^{6}Li and ^{7}Li lithium isotopes were recorded depending on the energies of deuterons and protons. Subsequent to the measurement results, the composition of the reduced ZrO_2 powder corresponded to the formula $Li_{0.87}ZrO_{1.98}$ with an error in determining the indices of lithium and oxygen within 2%–3%. Based on the results of the NRA, the following conclusions can be made:

- the mass fraction of oxygen in the reduced ZrO_2 can only act as an estimated measure of the course of the reduction process, since the reduction reaction is accompanied by the formation of compounds with a high concentration of lithium;
- the mass fraction of oxygen in the reduced ZrO_2 was 24.6 ± 1.0 wt%, that is the decrease in the mass fraction of oxygen was insignificant in comparison with the initial compound ZrO_2, in which it was 26 wt%;
- the mass fraction of lithium in the reduced ZrO_2 was 4.76 ± 0.19 wt%;
- the valence of zirconium significantly changed and the reduction of ZrO_2 occurred.

The formula for the reduction product can mean that the obtained powder is one of the mixtures: Zr_2O_3 [41,42] and Li_2O; ZrO and Li_2ZrO_3; Zr, zirconium oxides and lithium zirconates.

Despite an obvious fact of the ZrO_2 reduction by lithium, the methods used in this study and in previous works are not the basis for an accurate determination of the reduction degree of oxide and

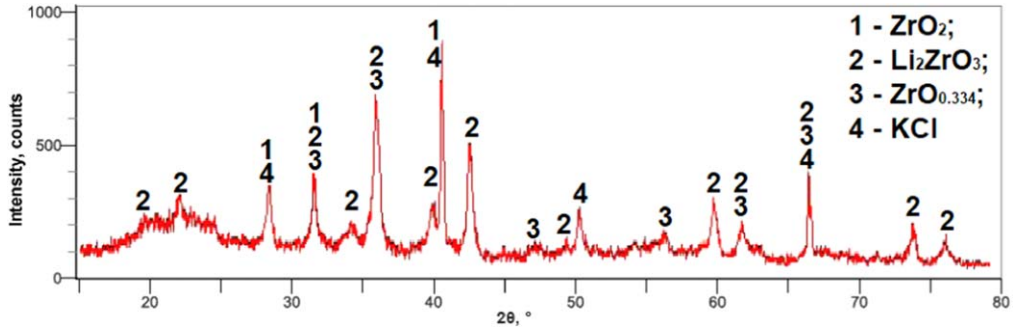

Figure 9. The diffraction pattern of ZrO_2 powder reduced by lithium during the long-term electrolysis of the LiCl-KCl-(1.5 wt%)Li_2O melt at 650 °C.

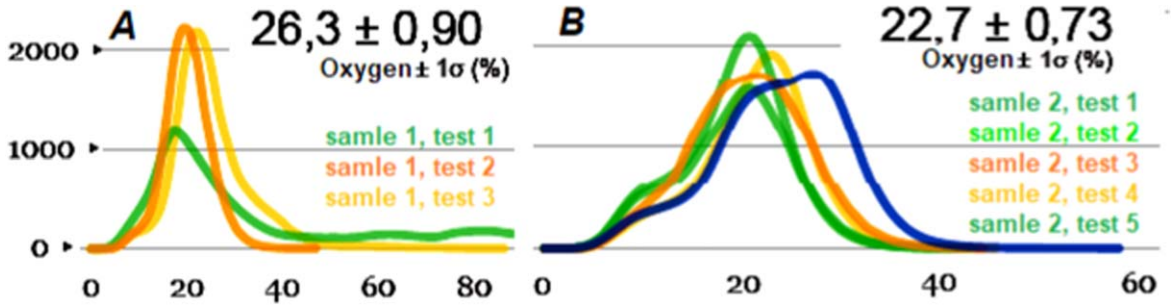

Figure 10. The oxygen content according to LECO analyzer data in ZrO_2 powder before and after the reduction during electrolysis in the LiCl-KCl-(1.5 wt%) Li_2O melt.

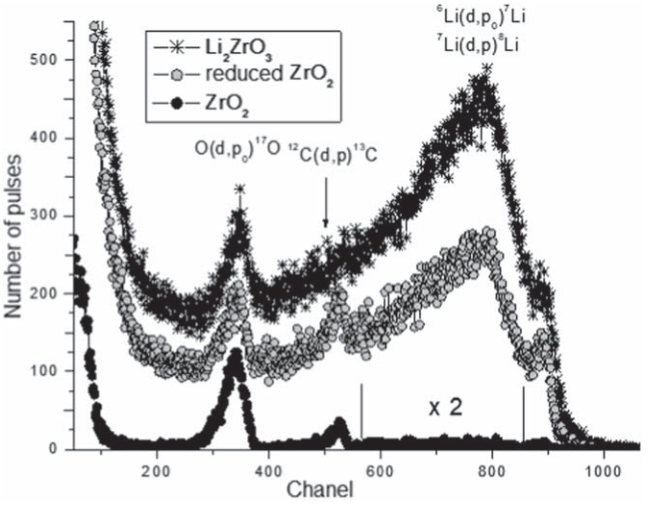

Figure 11. The spectra of nuclear reactions of the studied powders.

intermediate lithium zirconates to metallic zirconium. Moreover, as noted in the introduction chapter and according to the electrochemical measurements, the appearance of zirconium in reduction products can be associated with direct electroreduction of dissolved zirconium ions, following the reaction:[2]

$$Zr^{4+} + ze^- = Zr^{(4-z)+} (z = 1 - 4) \quad [4]$$

or electro-deoxidation of ZrO_2 by reactions, for example:[21]

$$xZrO_2 + 2(2x - 1)e - = Zr_xO + (2x - 1)O^{2-} \quad [5]$$

$$Zr_xO + 2e^- = xZr + O^{2-} \quad [6]$$

Based on the electrochemical measurements described above, the most probable is the reduction of zirconium by a diffusion-controlled reaction (4), since the processes (5) and (6) are limited by the removal of lithium oxide from the pores of the reduced oxide.

Table I. Elemental composition (wt%) of tin after melting with the ZrO_2, Li_2ZrO_3, and the ZrO_2 reduction products.

	Element composition, wt%				
Sample	K	Li	Fe	Mo	Zr
Sn	0.030	0.002	0.009	<0.0004	0.0001
Sn + ZrO_2	0.021	0.001	0.011	<0.0001	0.0001
Sn + Li_2ZrO_3	0.024	0.002	0.010	<0.0001	0.0002
Sn + reduced ZrO_2	0.030	0.007	0.020	<0.0001	0.0007

Alloying with tin.—In order to estimate the zirconium content in reduction products an approach was applied,[30] which included melting the product with a metal that forms alloys and intermetallic compounds with zirconium, but does not reduce ZrO_2 and lithium zirconates. In the present work, the tin[43] (weight 35 g) was chosen as the alloy-forming metal, with which the following components were melted: the initial ZrO_2, the lithium zirconate, and the ZrO_2 reduction product washed out of salts (3 g each). The elemental composition of the tin after melting is listed in Table I.

According to the results shown in Table I, it can be seen that the proportion of zirconium in the tin increased by 0.0006 wt%; this indicates that the degree of ZrO_2 reduction to the metallic zirconium does not exceed 0.0001%. These observations are differed from the results obtained during the study of the ZrO_2 reduction in the LiCl-Li_2O melt.[11–14] Moreover, a detailed attention should be paid to the reduction of ZrO_2 and its mixtures with actinide oxides when developing the schemes for the SNF pyrochemical reprocessing.

Conclusions

Zirconium oxide is one of the main by-products in the pyrochemical reprocessing of the spent nuclear fuel, and data related to

the zirconium separation during reduction of actinide oxides seem to be very important for studying subsequent stages of processing.

In the present work, using a set of electrochemical methods, the effect of ZrO_2 in the space near the cathode on the regularities of the cathode process on molybdenum in the LiCl-KCl-(1.5 wt%)Li_2O melt at 650 °C was studied. It was revealed that the appearance of ZrO_2 in the cathode space led to the consumption of released lithium and increase in the potential relaxation time of molybdenum cathode in the ZrO_2 powder after its short-term polarization. These observations indicate the reduction of ZrO_2 by lithium. Based on the literature data the rate of this process can be considered as low in comparison with the rate of the UO_2 reduction by lithium.

The reduction of ZrO_2 by lithium in the course of long-term galvanic impulse electrolysis yielded a dark gray powder, presented by the phases ZrO_2, Li_2ZrO_3, Zr_3O, and KCl. The consistent ZrO_2 reduction was confirmed by direct physicochemical methods, as well as by nuclear microanalysis. At the same time, no reduction to metallic zirconium was observed. Possible reasons of the previous detection of the metallic zirconium in the products of ZrO_2 reduction by lithium during electrolysis of the LiCl-Li_2O melts were considered.

Acknowledgments

The work was carried out within the state assignment of Ministry of Sciences and Higher Education of Russian Federation (theme No AAAA-A16-116051110162-3). Nuclear reaction analysis was performed at the Institute of Metal Physics of the UB RAS within the state assignment of Ministry of Sciences and Higher Education of Russian Federation (theme "Function" No AAAA-A19-119012990095-0). Atomic emission analysis was conducted on the equipment of the Composition of Compounds the Shared Access Centre of the Institute of High Temperature Electrochemistry of the UB RAS.

ORCID

Andrey Suzdaltsev https://orcid.org/0000-0003-3004-7611

References

1. A. N. Baraboshkin, *Electrocrystallizatoin of metals from molten salts* (Nauka, Moscow) (1976).
2. M. V. Smirnov, *Electrode potentials in molten chlorides* (Nauka, Moscow) (1973).
3. M. Gaune-Escard and G. M. Haarberg (ed.), *Molten Salts Chemistry and Technology* (John Wiley & Sons, Ltd)(USA) (2014).
4. T. Inoue and L. Koch, *Nucl. Eng. & Tech.*, **40**, 183 (2008).
5. J. L. Willit, W. E. Miller, and J. E. Battles, *J. Nucl. Mat.*, **195**, 229 (1992).
6. K. Nagarajan et al., *Energy Procedia*, **7**, 431 (2011).
7. Y. P. Zaikov, V. Y. Shishkin, A. M. Potapov, A. E. Dedyukhin, V. A. Kovrov, A. S. Kholkina, V. A. Volkovich, and I. B. Polovov, *J. of Physics: Conf. Series,*, **1475**, 012027 (2020).
8. S. P. Fusselman et al., *J. Electrochem. Soc.*, **146**, 2573 (1999).
9. A. Merwin, M. A. Williamson, J. L. Willit, and D. Chidambaram, *J. Electrochem. Soc.*, **164**, H5236 (2017).
10. E.-Y. Choi, J. Lee, D. H. Heo, S. K. Lee, M. K. Jeon, S. S. Hong, S.-W. Kim, H. W. Kang, S.-C. Jeon, and J.-M. Hur, *J. Nucl. Mat.*, **489**, 1 (2017).
11. Y. Sakamura, M. Iizuka, S. Kitawaki, A. Nakayoshi, and H. Kofuji, *J. Nucl. Mat.*, **466**, 269 (2015).
12. E.-Y. Choi and D. H. Heo, *J. Nucl. Mat.*, **512**, 193 (2018).
13. K. S. Mohandas, N. Sanil, and L. Shakila, *J. Nucl. Mat.*, **521**, 109 (2019).
14. E.-Y. Choi, M. K. Jeon, S.-W. Kim, and S. Paek, *J. Nucl. Mat.*, **533**, 152107 (2020).
15. S. H. Cho, D. Y. Kim, S. Kwon, B. H. Yoon, and J. H. Lee, *J. Nucl. Sci. & Tech.*, **55**, 97 (2018).
16. S. H. Cho, S. B. Park, J. H. Lee, J. M. Hur, and H. S. Lee, *Mat. Chem. & Phys.*, **131**, 743 (2012).
17. M. Takeuchi, T. Kato, and K. Hanada, *J. Phys. Chem. Solids*, **66**, 521 (2005).
18. A. I. Valtseva, P. S. Pershin, A. V. Suzdaltsev, and Y. P. Zaikov, *J. of Phys.: Conf. Series*, **1683**, 032029 (2020).
19. N. D. Shikina, O. N. Vasina, E. V. Gurova, E. S. Popova, B. R. Tagirov, Y. K. Shazzo, and I. L. Khodakovskii, *Geochem. Int.*, **52**, 82 (2014).
20. P. L. Brown, E. Curty, and B. Grambow, *Chemical Thermodynamics of Zirconium* (Elsevier, Nuclear Energy Agency) (2005).
21. X. Ping, K. Liu, Y. Liu, L. Yuan, B. Yao, X. Zhao, Z. Chai, and W. Shi, *J. Electrochem. Soc.*, **164**, D888 (2017).
22. J. Peng, G. Li, H. Chen, D. Wang, X. Jin, and G. Z. Chen, *J. Electrochem. Soc.*, **157**, F1 (2010).
23. N. I. Shurov, A. P. Khramov, Y. P. Zaikov, V. A. Kovrov, and A. V. Suzdaltsev, *Rus. J. Non-ferrous Metals*, **56**, 267 (2015).
24. V. Yu. Shishkin and V. S. Mityaev, *Izvestiya AN USSR. Neorganicheskie Materialy*, **1982**, 1917 (1982).
25. A. Mullabaev, O. Tkacheva, V. Shishkin, V. Kovrov, Y. Zaikov, L. Sukhanov, and Y. Mochalov, *J. Nucl. Mat.*, **500**, 235 (2018).
26. S. K. Cho, S.-K. Lee, E.-Y. Choi, and J.-M. Hur, *J. Electrochem. Soc.*, **163**, E308 (2016).
27. V. N. Volkov, V. B. Vykhodets, I. K. Golubkov, S. M. Klotsman, P. V. Lerkh, and V. A. Pavlov, *Nucl. Instrum. Methods*, **205**, 73 (1983).
28. V. B. Vykhodets, S. M. Klotsman, and A. D. Levin, *Metallography*, **64**, 920 (1987).
29. I. A. Anokhina, I. E. Animitsa, V. I. Voronin, V. B. Vykhodets, T. E. Kurennykh, N. G. Molchanova, A. I. Vylkov, A. E. Dedyukhin, and Y. P. Zaikov, *Cer. Int.*, **47**, 1949 (2021).
30. A. Y. Nikolaev, A. V. Suzdaltsev, and Y. P. Zaikov, *J. Electrochem. Soc.*, **166**, D252 (2019).
31. S. Ghosh, S. Vandarkuzhali, P. Venkatesh, G. Seenivasan, T. Subramanian, B. Prabhakara Reddy, and K. Nagarajan, *J. Electroanal. Chem.*, **627**, 15 (2009).
32. Y. Sakamura, *J. Electrochem. Soc*, **151**, C187 (2004).
33. W. Han, W. Wang, M. Li, J. Wang, Y. Sun, X. Yang, and M. Zhang, *Sep. & Purif. Techn.*, **232**, 115965 (2020).
34. V. A. Volkovich, D. S. Maltsev, M. N. Soldatova, A. A. Ryzhov, A. B. Ivanov, and E. C. S. Trans, **98**, 355 (2020).
35. Y. Ma, T. Yamamoto, K. Yasuda, and T. Nohira, *ECS. Trans*, **98**, 215 (2020).
36. W. Park, J.-M. Hur, E.-Y. Choi, and J.-K. Kim, *J. Korean Radioact. Waste Soc.*,, **10**, 229 (2012).
37. A. V. Suzdaltsev, A. P. Khramov, Y. P. Zaikov, A. A. Pankratov, E. G. Vovkotrub, and B. D. Antonov, *J. Electrochem. Soc.*, **164**, H5183 (2017).
38. V. Afonichkin, A. Bovet, and V. Shishkin, *J. Nucl. Mat.*, **419**, 347 (2011).
39. E.-Y. Choi, C. Y. Won, D.-S. Kang, S.-W. Kim, J.-S. Cha, S.-J. Lee, W. Park, H. S. Im, and J.-M. Hur, *J. Radioanal. Nucl. Chem*, **304**, 535 (2015).
40. W. Park, E.-Y. Choi, S.-W. Kim, S.-C. Jeon, Y.-H. Cho, and J.-M. Hur, *J. Nucl. Mat.*, **477**, 59 (2016).
41. Z. Ma, J. Zhang, G. Yan, H. Liu, J. Huang, and L. Wang, *J. Alloys & Comp*, **810**, 151964 (2019).
42. B. Puchala and A. Van Der Ven, *Phys. Review B*, **88**, 094108 (2013).
43. V. I. Baykov, R. J. Perez, P. A. Korzhavyi, B. Sundman, and B. Johansson, *Scripta Materialia*, **55**, 485 (2006).